8-31-2017

Space Telescope and Optical Reverberation Mapping Project. VII. Understanding the Ultraviolet Anomaly in NGC 5548 with X-Ray Spectroscopy

S. Mathur
The Ohio State University

A. Gupta
The Ohio State University

K. Page
University of Leicester, UK

R. W. Pogge
The Ohio State University

Y. Krongold
Universidad Nacional Autonoma de Mexico, Mexico

See next page for additional authors

Authors
S. Mathur, A. Gupta, K. Page, R. W. Pogge, Y. Krongold, M. R. Goad, S. M. Adams, M. D. Anderson, P. Arévalo, A. J. Barth, C. Bazhaw, T. G. Beatty, M. C. Bentz, A. Bigley, S. Bisogni, G. A. Borman, T. A. Boroson, M. C. Bottorff, W. N. Brandt, A. A. Breeveld, J. E. Brown, J. S. Brown, E. M. Cackett, G. Canalizo, M. T. Carini, K. I. Clubb, J. M. Comerford, C. T. Coker, E. M. Corsini, D. M. Crenshaw, and Gary J. Ferland

Space Telescope and Optical Reverberation Mapping Project. VII. Understanding the Ultraviolet Anomaly in NGC 5548 with X-Ray Spectroscopy

Notes/Citation Information
Published in *The Astrophysical Journal*, v. 846, no. 1, 55, p. 1-9.

Due to the large number of authors, only the first 30 and the authors affiliated with the University of Kentucky are listed in the author section above. For the complete list of authors, please download this article.

Digital Object Identifier (DOI)
https://doi.org/10.3847/1538-4357/aa832b

The Astrophysical Journal, 846:55 (9pp), 2017 September 1 https://doi.org/10.3847/1538-4357/aa832b

Space Telescope and Optical Reverberation Mapping Project. VII. Understanding the Ultraviolet Anomaly in NGC 5548 with X-Ray Spectroscopy

S. Mathur[1,2], A. Gupta[2,3], K. Page[4], R. W. Pogge[1,2], Y. Krongold[5], M. R. Goad[4], S. M. Adams[1,6], M. D. Anderson[7], P. Arévalo[8], A. J. Barth[9], C. Bazhaw[7], T. G. Beatty[1,10,11], M. C. Bentz[7], A. Bigley[12], S. Bisogni[1,13], G. A. Borman[14], T. A. Boroson[15], M. C. Bottorff[16], W. N. Brandt[10,17,18], A. A. Breeveld[19], J. E. Brown[20], J. S. Brown[1], E. M. Cackett[21], G. Canalizo[22], M. T. Carini[23], K. I. Clubb[12], J. M. Comerford[24], C. T. Coker[1], E. M. Corsini[25,26], D. M. Crenshaw[7], S. Croft[12], K. V. Croxall[1,2,27], E. Dalla Bontà[25,26], A. J. Deason[28,29], K. D. Denney[1,2,27,88], A. De Lorenzo-Cáceres[30], G. De Rosa[1,2,31], M. Dietrich[32], R. Edelson[33], J. Ely[31], M. Eracleous[10,17], P. A. Evans[4], M. M. Fausnaugh[1], G. J. Ferland[34], A. V. Filippenko[12], K. Flatland[35], O. D. Fox[12,31], E. L. Gates[36], N. Gehrels[37], S. Geier[38,39,40], J. M. Gelbord[41,42], V. Gorjian[43], J. E. Greene[44], C. J. Grier[10,17], D. Grupe[45], P. B. Hall[46], C. B. Henderson[1,43,89], S. Hicks[23], E. Holmbeck[47], T. W.-S. Holoien[1,2], D. Horenstein[7], Keith Horne[30], T. Hutchison[16], M. Im[48], J. J. Jensen[49], C. A. Johnson[50], M. D. Joner[51], J. Jones[7], J. Kaastra[52,53,54], S. Kaspi[55,56], B. C. Kelly[57], P. L. Kelly[58,59,60], J. A. Kennea[10], M. Kim[61], S. Kim[1,2], S. C. Kim[61], A. King[62], S. A. Klimanov[63], C. S. Kochanek[1,2], K. T. Korista[64], G. A. Kriss[31,65], M. W. Lau[28], J. C. Lee[61], D. C. Leonard[35], M. Li[66], P. Lira[67], Z. Ma[20], F. MacInnis[16], E. R. Manne-Nicholas[7], M. A. Malkan[47], J. C. Mauerhan[12], R. McGurk[28,68], I. M. McHardy[69], C. Montouri[70], L. Morelli[25,26], A. Mosquera[1,71], D. Mudd[1], F. Muller-Sanchez[24], R. Musso[16], S. V. Nazarov[14], H. Netzer[55], M. L. Nguyen[72], R. P. Norris[7], J. A. Nousek[10], P. Ochner[25,26], D. N. Okhmat[14], B. Ou-Yang[7], A. Pancoast[73,90], I. Papadakis[74,75], J. R. Parks[7], L. Pei[9,76], B. M. Peterson[1,2,31], A. Pizzella[25,26], R. Poleski[1], J.-U. Pott[68], S. E. Rafter[56,77], H.-W. Rix[68], J. Runnoe[10,17,78], D. A. Saylor[7], J. S. Schimoia[1,79], K. Schnülle[68], S. G. Sergeev[14], B. J. Shappee[1,80,91], I. Shivvers[12], M. Siegel[15], G. V. Simonian[1], A. Siviero[25], A. Skielboe[49], G. Somers[1,81], M. Spencer[51], D. Starkey[30], D. J. Stevens[1], H.-I. Sung[61], J. Tayar[1], N. Tejos[82,83], C. S. Turner[7], P. Uttley[84], J. Van Saders[80], M. Vestergaard[49,85], L. Vican[47], S. Villanueva Jr.[1], C. Villforth[30,86], Y. Weiss[56], J.-H. Woo[48], H. Yan[20], S. Young[33], H. Yuk[12,87], W. Zheng[12], W. Zhu[1], and Y. Zu[2]

[1] Department of Astronomy, The Ohio State University, 140 West 18th Avenue, Columbus, OH 43210, USA
[2] Center for Cosmology and AstroParticle Physics, The Ohio State University, 191 West Woodruff Avenue, Columbus, OH 43210, USA
[3] Department of Biological and Physical Sciences, Columbus State Community College, Columbus, OH 43215, USA
[4] Department of Physics and Astronomy, University of Leicester, Leicester, LE1 7RH, UK
[5] Instituto de Astronomia, Universidad Nacional Autonoma de Mexico, Cuidad de Mexico, Mexico
[6] Cahill Center for Astrophysics, California Institute of Technology, Pasadena, CA 91125, USA
[7] Department of Physics and Astronomy, Georgia State University, 25 Park Place, Suite 605, Atlanta, GA 30303, USA
[8] Instituto de Física y Astronomía, Facultad de Ciencias, Universidad de Valparaíso, Gran Bretana N 1111, Playa Ancha, Valparaíso, Chile
[9] Department of Physics and Astronomy, 4129 Frederick Reines Hall, University of California, Irvine, CA 92697, USA
[10] Department of Astronomy and Astrophysics, Eberly College of Science, The Pennsylvania State University, 525 Davey Laboratory, University Park, PA 16802, USA
[11] Center for Exoplanets and Habitable Worlds, The Pennsylvania State University, University Park, PA 16802, USA
[12] Department of Astronomy, University of California, Berkeley, CA 94720-3411, USA
[13] Osservatorio Astrofisico di Arcetri, largo E. Fermi 5, I-50125, Firenze, Italy
[14] Crimean Astrophysical Observatory, P/O Nauchny, Crimea 298409, Russia
[15] Las Cumbres Observatory Global Telescope Network, 6740 Cortona Drive, Suite 102, Goleta, CA 93117, USA
[16] Fountainwood Observatory, Department of Physics FJS 149, Southwestern University, 1011 East University Avenue, Georgetown, TX 78626, USA
[17] Institute for Gravitation and the Cosmos, The Pennsylvania State University, University Park, PA 16802, USA
[18] Department of Physics, 104 Davey Laboratory, The Pennsylvania State University, University Park, PA 16802, USA
[19] Mullard Space Science Laboratory, University College London, Holmbury St. Mary, Dorking, Surrey RH5 6NT, UK
[20] Department of Physics and Astronomy, University of Missouri, Columbia, MO 65211, USA
[21] Department of Physics and Astronomy, Wayne State University, 666 West Hancock Street, Detroit, MI 48201, USA
[22] Department of Physics and Astronomy, University of California, Riverside, CA 92521, USA
[23] Department of Physics and Astronomy, Western Kentucky University, 1906 College Heights Boulevard #11077, Bowling Green, KY 42101, USA
[24] Department of Astrophysical and Planetary Sciences, University of Colorado, Boulder, CO 80309, USA
[25] Dipartimento di Fisica e Astronomia "G. Galilei," Università di Padova, Vicolo dell'Osservatorio 3, I-35122 Padova, Italy
[26] INAF-Osservatorio Astronomico di Padova, Vicolo dell'Osservatorio 5 I-35122, Padova, Italy
[27] Illumination Works, LLC, 5650 Blazer Parkway, Dublin, OH 43017, USA
[28] Department of Astronomy and Astrophysics, University of California Santa Cruz, 1156 High Street, Santa Cruz, CA 95064, USA
[29] Institute for Computational Cosmology, Department of Physics, University of Durham, South Road, Durham DH1 3LE, UK
[30] SUPA Physics and Astronomy, University of St. Andrews, Fife, KY16 9SS Scotland, UK
[31] Space Telescope Science Institute, 3700 San Martin Drive, Baltimore, MD 21218, USA
[32] Department of Earth, Environment and Physics, Worcester State University, Worcester, MA 01602, USA
[33] Department of Astronomy, University of Maryland, College Park, MD 20742, USA
[34] Department of Physics and Astronomy, The University of Kentucky, Lexington, KY 40506, USA
[35] Department of Astronomy, San Diego State University, San Diego, CA 92182, USA
[36] Lick Observatory, P.O. Box 85, Mt. Hamilton, CA 95140, USA
[37] Astrophysics Science Division, NASA Goddard Space Flight Center, Mail Code 661, Greenbelt, MD 20771, USA
[38] Instituto de Astrofísica de Canarias, E-38200 La Laguna, Tenerife, Spain
[39] Departamento de Astrofísica, Universidad de La Laguna, E-38206 La Laguna, Tenerife, Spain
[40] Gran Telescopio Canarias (GRANTECAN), 38205 San Cristóbal de La Laguna, Tenerife, Spain
[41] Spectral Sciences Inc., 4 Fourth Avenue, Burlington, MA 01803, USA
[42] Eureka Scientific Inc., 2452 Delmer Street Suite 100, Oakland, CA 94602, USA

[43] Jet Propulsion Laboratory, California Institute of Technology, 4800 Oak Grove Drive, Pasadena, CA 91109, USA
[44] Department of Astrophysical Sciences, Princeton University, Princeton, NJ 08544, USA
[45] Space Science Center, Morehead State University, 235 Martindale Drive, Morehead, KY 40351, USA
[46] Department of Physics and Astronomy, York University, Toronto, ON M3J 1P3, Canada
[47] Department of Physics and Astronomy, University of California, Los Angeles, CA 90095, USA
[48] Astronomy Program, Department of Physics & Astronomy, Seoul National University, Seoul, Korea
[49] Dark Cosmology Centre, Niels Bohr Institute, University of Copenhagen, Juliane Maries Vej 30, DK-2100 Copenhagen Ø, Denmark
[50] Santa Cruz Institute for Particle Physics and Department of Physics, University of California, Santa Cruz, CA 95064, USA
[51] Department of Physics and Astronomy, N283 ESC, Brigham Young University, Provo, UT 84602, USA
[52] SRON Netherlands Institute for Space Research, Sorbonnelaan 2, 3584 CA Utrecht, The Netherlands
[53] Department of Physics and Astronomy, Univeristeit Utrecht, P.O. Box 80000, 3508 Utrecht, The Netherlands
[54] Leiden Observatory, Leiden University, P.O. Box 9513, 2300 RA Leiden, The Netherlands
[55] School of Physics and Astronomy, Raymond and Beverly Sackler Faculty of Exact Sciences, Tel Aviv University, Tel Aviv 69978, Israel
[56] Physics Department, Technion, Haifa 32000, Israel
[57] Department of Physics, University of California, Santa Barbara, CA 93106, USA
[58] Department of Physics, Stanford University, 382 Via Pueblo Mall, Stanford, CA 94305, USA
[59] Kavli Institute for Particle Astrophysics and Cosmology, Stanford University, Stanford, CA 94305, USA
[60] SLAC National Accelerator Laboratory, 2575 Sand Hill Road, Menlo Park, CA 94025, USA
[61] Korea Astronomy and Space Science Institute, Korea
[62] School of Physics, University of Melbourne, Parkville, VIC 3010, Australia
[63] Pulkovo Observatory, 196140 St. Petersburg, Russia
[64] Department of Physics, Western Michigan University, 1120 Everett Tower, Kalamazoo, MI 49008-5252, USA
[65] Department of Physics and Astronomy, The Johns Hopkins University, Baltimore, MD 21218, USA
[66] Department of Astronomy, Columbia University, 550 West 120th Street, New York, NY 10027, USA
[67] Departamento de Astronomia, Universidad de Chile, Camino del Observatorio 1515, Santiago, Chile
[68] Max Planck Institut für Astronomie, Königstuhl 17, D-69117 Heidelberg, Germany
[69] University of Southampton, Highfield, Southampton, SO17 1BJ, UK
[70] DiSAT, Universita dell'Insubria, via Valleggio 11, I-22100, Como, Italy
[71] Physics Department, United States Naval Academy, Annapolis, MD 21403, USA
[72] Department of Physics and Astronomy, University of Wyoming, 1000 E. University Avenue, Laramie, WY 82071, USA
[73] Harvard-Smithsonian Center for Astrophysics, 60 Garden Street, Cambridge, MA 02138, USA
[74] Department of Physics and Institute of Theoretical and Computational Physics, University of Crete, GR-71003 Heraklion, Greece
[75] IESL, Foundation for Research and Technology, GR-71110 Heraklion, Greece
[76] Department of Astronomy, University of Illinois at Urbana-Champaign, Urbana, IL 61801, USA
[77] Department of Physics, Faculty of Natural Sciences, University of Haifa, Haifa 31905, Israel
[78] Department of Astronomy, University of Michigan, 1085 S. University Avenue, Ann Arbor, MI 48109, USA
[79] Instituto de Física, Universidade Federal do Rio do Sul, Campus do Vale, Porto Alegre, Brazil
[80] Carnegie Observatories, 813 Santa Barbara Street, Pasadena, CA 91101, USA
[81] Department of Physics and Astronomy, Vanderbilt University, 6301 Stevenson Circle, Nashville, TN 37235, USA
[82] Millennium Institute of Astrophysics, Santiago, Chile
[83] Instituto de Astrofísica, Pontificia Universidad Católica de Chile, Vicuña Mackenna 4860, Santiago, Chile
[84] Astronomical Institute "Anton Pannekoek," University of Amsterdam, Postbus 94249, NL-1090 GE Amsterdam, The Netherlands
[85] Steward Observatory, University of Arizona, 933 North Cherry Avenue, Tucson, AZ 85721, USA
[86] University of Bath, Department of Physics, Claverton Down, BA2 7AY, Bath, UK
[87] Department of Physics and Astronomy, San Francisco State University, 1600 Holloway Avenue, San Francisco, CA 94132, USA
Received 2017 April 20; revised 2017 July 27; accepted 2017 July 29; published 2017 August 31

Abstract

During the Space Telescope and Optical Reverberation Mapping Project observations of NGC 5548, the continuum and emission-line variability became decorrelated during the second half of the six-month-long observing campaign. Here we present *Swift* and *Chandra* X-ray spectra of NGC 5548 obtained as part of the campaign. The *Swift* spectra show that excess flux (relative to a power-law continuum) in the soft X-ray band appears before the start of the anomalous emission-line behavior, peaks during the period of the anomaly, and then declines. This is a model-independent result suggesting that the soft excess is related to the anomaly. We divide the *Swift* data into on- and off-anomaly spectra to characterize the soft excess via spectral fitting. The cause of the spectral differences is likely due to a change in the intrinsic spectrum rather than to variable obscuration or partial covering. The *Chandra* spectra have lower signal-to-noise ratios, but are consistent with the *Swift* data. Our preferred model of the soft excess is emission from an optically thick, warm Comptonizing corona, the effective optical depth of which increases during the anomaly. This model simultaneously explains all three observations: the UV emission-line flux decrease, the soft-excess increase, and the emission-line anomaly.

Key words: galaxies: active – galaxies: individual (NGC 5548) – X-rays: galaxies – X-rays: individual (NGC 5548)

1. Introduction

The Space Telescope and Optical Reverberation Mapping (STORM) project intensively monitored the well-known active galactic nucleus (AGN) NGC 5548. As part of this project, NGC 5548 was observed with the *Hubble Space Telescope*

[88] NSF Postdoctoral Research Fellow.
[89] NASA Postdoctoral Program Fellow.
[90] Einstein Fellow.
[91] Carnegie-Princeton Fellow, Hubble Fellow.

(*HST*) in 2014 for 180 days with a daily cadence, obtaining 171 usable epochs. The source was also monitored with *Swift* and in the optical with ground-based observations. In addition, we observed the source with *Chandra* four times during the *HST* observing campaign. The goal of the STORM project was to perform velocity-resolved reverberation mapping (RM) of the optical and ultraviolet (UV) emission lines with fine time sampling, long duration, and high signal-to-noise ratio (S/N) spectra. The multiwavelength continuum observations were performed to probe the structure of the accretion disk and to track changes in the ionizing continuum of the source.

The *HST* (UV), *Swift* (X-ray), and ground-based (optical) continuum and spectroscopic observations are presented in Papers I–V (De Rosa et al. 2015; Edelson et al. 2015; Fausnaugh et al. 2016; Goad et al. 2016, and Pei et al. 2017, respectively). Reverberating-disk models for NGC 5548 are presented in Paper VI (Starkey et al. 2017). As noted in Paper I and discussed in detail in Paper IV (Goad et al. 2016), an anomalous behavior of the broad UV emission lines was observed during the campaign. For most of the campaign, the broad UV emission lines responded to changes in the UV continuum, as generally expected for broad-line reverberation. However, there was a period of 60–70 days during the latter half of the campaign when the UV lines did not reverberate with the UV continuum. This was also accompanied by a significant drop in the fluxes and equivalent widths of UV and optical emission lines, to varying degrees.

Such an "anomaly," when the continuum and emission-line variability became decoupled, was not previously observed in RM campaigns and demands explanation. Moreover, understanding the origin of the anomaly is critical to the robustness of the RM technique, since it depends on the observed continuum flux being a good proxy for the unobserved extreme-UV (EUV) ionizing continuum. Here we present X-ray spectra obtained as part of AGN STORM that provide important clues to the origin of the anomaly. In Section 2, we present analyses of *Swift* spectra. The *Chandra* observations and spectral analyses are presented in Section 3. In Section 4, we discuss how the appearance of a soft-X-ray excess a few days before the anomaly may clarify its origin. Although NGC 5548 was observed intensively with *XMM-Newton* in the years prior to the AGN STORM campaign (Kaastra et al. 2014; Mehdipour et al. 2015, 2016; Cappi et al. 2016), a detailed comparison with those data is beyond the scope of this paper. Here we focus on *Swift* and *Chandra* data obtained during our campaign.

2. *Swift* Observations

2.1. Spectra and Analysis

Descriptions of the *Swift* observations, data reduction, and time-series analysis are presented in Paper II. Here we present a time-resolved spectral analysis. In Figure 1, we show the 0.3–10.0 keV spectra in nine time bins, from pre-anomaly (days 1–54) to post-anomaly (days 150–170). The exposure times for each period are given in Table 1. We see that the hard X-ray continuum (2–10.0 keV) is constant over the period of the observation, but the soft X-ray flux (below ∼0.8 keV) increases from the pre-anomaly period (days 1–54) to days 55–75, peaks during days 75–85, and then fades during days 85–100. This is a model-independent result, suggesting that the soft excess is likely related to the anomaly. In Figure 2, we have reproduced Figure 1(e) from Paper IV; the black points show the percentage difference in the C IV flux. The red points show the percentage difference in count rate at ≈0.55 keV. This again shows that the soft excess increases on days 55–75, just before the start of the anomaly (on day ∼75), peaks during days 75–85, and then fades. This also shows that there is some delay of about 20 days between the period of high soft-excess and the period of the anomaly.

In order to perform the spectral modeling and to quantify the soft excess, we divided the *Swift* observations into two parts, which we call pre-anomaly and anomaly spectra (days 0.4 to 54.5 = JD 2, 456, 690.4189 to 2, 456, 744.5088, and days 55.4 to 84.9 = JD 2, 456, 745.3676 to 2, 456, 774.9165, respectively). A Galactic column density of $N_{\rm H} = 1.69 \times 10^{20}$ cm^{-2} (Dicky & Lockman 1990) was included in all the models. We simultaneously fitted both the spectra with an absorbed power-law model, adding a blackbody (BB) component to parameterize the soft excess. The parameters of the power-law slope (photon index Γ) and normalization were tied for the two spectra (as justified by Figure 1), but the intrinsic absorption and BB parameters were allowed to vary. The fit showed that the BB temperature is the same in the two spectra, so we tied the temperature and fitted the spectra again. The resulting fit was good ($\chi^2_\nu = 1.16$ for 1001 degrees of freedom).

In their model of the entire *XMM-Newton* observing campaign, Cappi et al. (2016) found an additional scattered soft X-ray component dominated by narrow emission lines, with 8% of the total soft X-ray flux. This soft component was constant over the whole campaign, so it cannot be responsible for the variable soft excess we see here. Nonetheless, we added a similar component to our model (XSPEC model apec) with flux as in Cappi et al. (2016) and found no improvement to the fit ($\chi^2_\nu = 1.16$ for 1001 degrees of freedom). The best-fit spectra are shown in Figure 3 and the model parameters are given in Table 2 along with the flux in the soft X-ray excess after correcting for absorption. The soft excess is significantly stronger in the anomaly spectrum. The intrinsic spectrum (without the instrument response) is shown in the bottom panel of Figure 3; the absorbed power law, BB, and scattered emission-line components are shown as dotted lines.

While a BB component describes the soft excess well, "warm Comptonization," in which seed photons from the accretion disk are Compton upscattered by an optically thick hotter corona is likely a more realistic model. Thus, we also tried to fit the soft excess with a warm Comptonization model (compTT in XSPEC), together with an absorbed power law. We fixed the model parameters (seed photon temperature, corona temperature, and optical depth) to the parameters in Mehdipour et al. (2015), allowing only the normalization to vary between the pre-anomaly and anomaly spectra. The resulting fit was worse ($\chi^2_\nu = 1.33$ for 1015 degrees of freedom; $\Delta\chi^2 = 189$ compared to the BB fit) and significant negative residuals were observed below 1 keV; in particular, the warm Comptonization model did not adequately fit the spectral turnover below 0.5 keV. We could improve the fit by adding another cold absorber at the source (best fit $N_{\rm H} = (4.7 \pm 0.7) \times 10^{20}$ cm^{-2}), resulting in $\chi^2_\nu = 1.2$ for 1014 degrees of freedom. Hence, if warm Comptonization is the correct description of the soft excess, it will have to lie behind this absorbing medium. The best-fit normalizations are

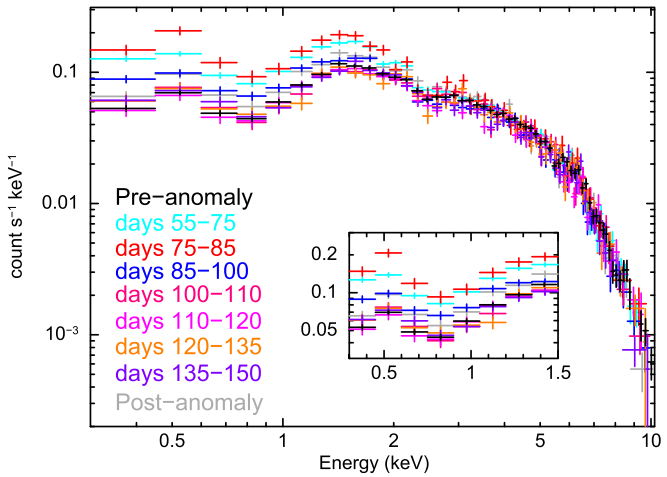

Figure 1. *Swift* spectra in different time bins. Note the increase in the soft excess from the pre-anomaly phase, peaking at days 75–85 (red) and then decreasing. This is a model-independent result, and suggests that the change in the spectral energy distribution of NGC 5548 is responsible for the anomaly. The inset shows 0.3 to 1.5 keV spectra for clarity.

Table 1
Swift Exposure Times

Days	Julian Dates	Exposure Time (ks)
0–55	2, 456, 690.4189–2, 456, 744.5088	58
55–75	2, 456, 745.3676–2, 456, 764.7642	32
75–85	2, 456, 765.6905–2, 456, 775.5760	7
85–100	2, 456, 776.0284–2, 456, 790.6312	20
100–110	2, 456, 791.0273–2, 456, 800.3587	12
110–120	2, 456, 800.8177–2, 456, 810.5546	14
120–135	2, 456, 810.8812–2, 456, 825.5525	10
135–150	2, 456, 825.9454–2, 456, 840.2837	16
150–170	2, 456, 840.2768–2, 456, 859.7580	15

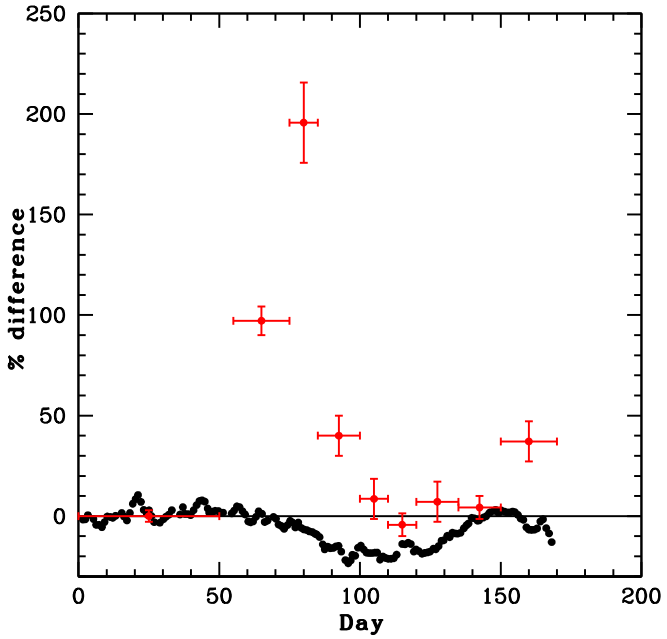

Figure 2. NGC 5548 light-curve. The black points show the percentage deficit in the C IV flux (reproduced from Figure 1(e) of Paper IV). This shows the onset of the anomaly around day 75 of the campaign. The red points show the percentage excess in the *Swift* count rate at ≈0.55 keV (as in Figure 1). We see that the soft excess increases before the start of the anomaly, peaks during the period of anomaly and then declines.

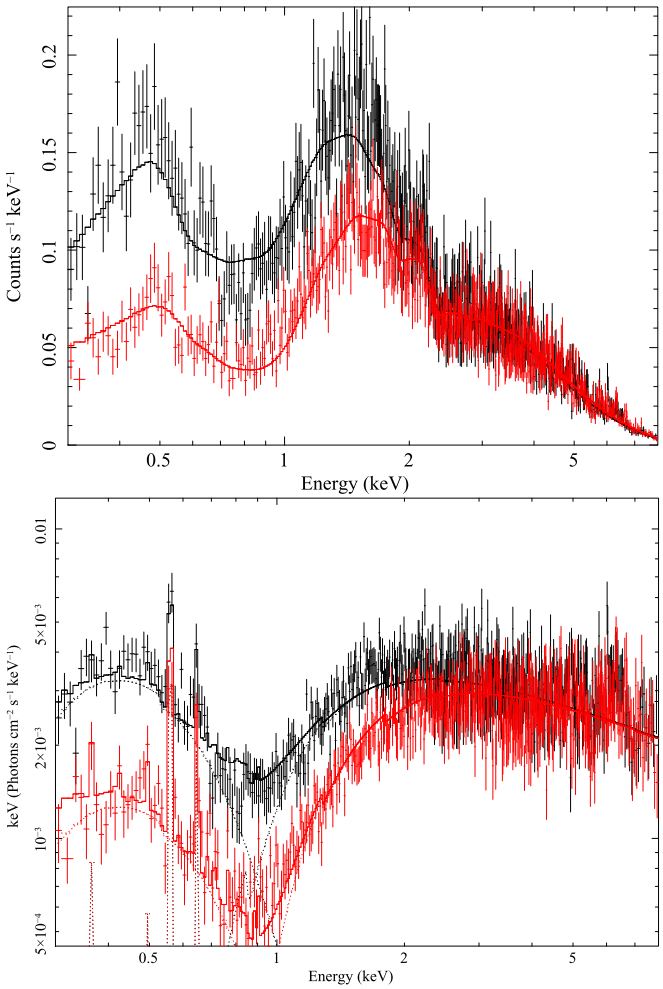

Figure 3. Top: *Swift* spectra: anomaly (black) and pre-anomaly (red) fit with an absorbed power law plus a blackbody model. An additional scattered component is also included. Bottom: the $Ef(E)$ intrinsic spectra (without folding in the instrument response); the three model components are shown as dotted lines.

given in Table 3 and the fit is shown in Figure 4; as expected, the normalization is significantly higher during the anomaly. Alternatively, the change in soft excess could be a result of a changing optical depth of the corona, as shown by Page et al. (2004). We therefore fixed the normalization to the pre-anomaly value and allowed only the optical depth to vary. As expected, we find significantly higher optical depth during the anomaly (Table 3). A warm Comptonized corona with variable optical depth is our preferred model for reasons discussed in Section 4.2.

When we fit the warm Comptonization model to the post-anomaly spectrum (days 150–170), the normalization is 29 ± 2 as compared to 22 ± 1 in the pre-anomaly spectrum and 50 ± 2 during the anomaly. At late times, the soft excess has dropped significantly and is close to the excess in the early phase. While there is some delay with respect to the emission-line anomaly and the continuum transitions are not very sharp (as we see in Figure 1), this strengthens our assertion that the increase in the soft-excess is likely the cause of the anomaly. For the rest of the paper, we focus only on spectra before and during the anomaly.

Table 2
Fits to *Swift* Spectra: Absorbed Power-law Plus Blackbody Model[a,c]

Obs ID	BB (kT)[b] keV	BB Norm 10^{-5} ph keV^{-1} s^{-1} cm^{-2}	BB Flux 0.1–2 keV 10^{-12} erg cm^{-2} s^{-1}	Intrinsic Absorption $N_{\rm H}$ 10^{22} cm^{-2}	Photon Index[b] Γ	Power-law Norm[b] 10^{-3} ph keV^{-1} s^{-1} cm^{-2}
Anomaly	0.12 ± 0.005	4.5 ± 0.2	3.7	0.66 ± 0.05	1.49 ± 0.04	5.9 ± 0.3
Pre-anomaly	0.12 ± 0.005	1.7 ± 0.1	1.4	1.13 ± 0.06	1.49 ± 0.04	5.9 ± 0.3

Notes.
[a] A scattered component is also included in the fit (see the text).
[b] Power-law parameters and BB temperature are tied for both the data sets.
[c] χ^2_ν for the joint fit is 1.16 for $\nu = 1001$ degrees of freedom.

Table 3
Swift Spectra: Warm Comptonization Fit Parameters[a,b]

Spectrum	Optical Depth	Normalization
Anomaly	22.34 ± 0.16	50.34 ± 1.85
Pre-anomaly	20.55 ± 0.15	22.09 ± 0.94

Notes.
[a] Power-law parameters are tied for both the data sets.
[b] The warm corona temperature was fixed at 0.15 keV and the seed photon temperature to 0.74 eV. Only one parameter (optical depth or normalization) was allowed to vary at a time.

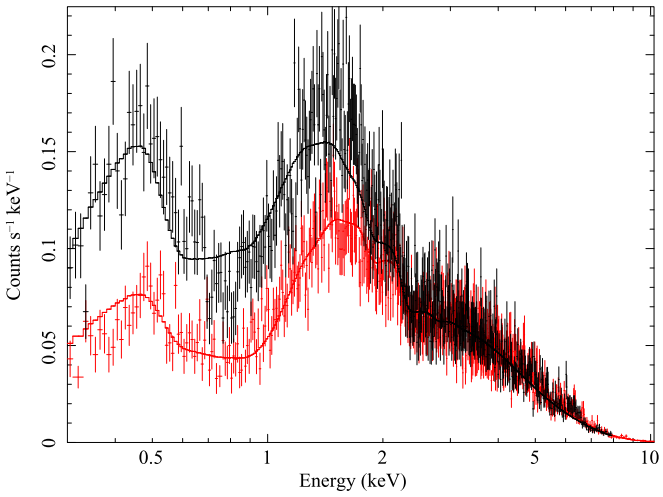

Figure 4. As in Figure 3, but fit with a warm Comptonization model.

2.2. Alternative Models

It is possible that the observed spectral shape (the "soft excess") is an artifact of a partially covering cold absorber. We therefore tried to fit the soft excess with a partial covering power-law model. The best-fit absorption column densities in the two spectra were found to be the same within the uncertainties, so we refitted the two spectra after tying the column densities. As expected, the absorber covered the continuum source more during the pre-anomaly period (covering fraction 0.91 ± 0.01) and less during the anomaly (covering fraction 0.75 ± 0.02). However, this fit is worse ($\chi^2_\nu = 1.4$ for 1003 degrees of freedom) than the BB model, with obvious residuals in the soft X-ray spectrum. As seen in Figure 5, the partial covering absorber model does not adequately account for the excess flux in the soft X-ray band in the anomaly spectrum, or the spectral turnover below $\sim$2 keV. Thus, the dominant parameter describing the change in soft excess between pre-anomaly and anomaly spectra cannot be the covering factor.

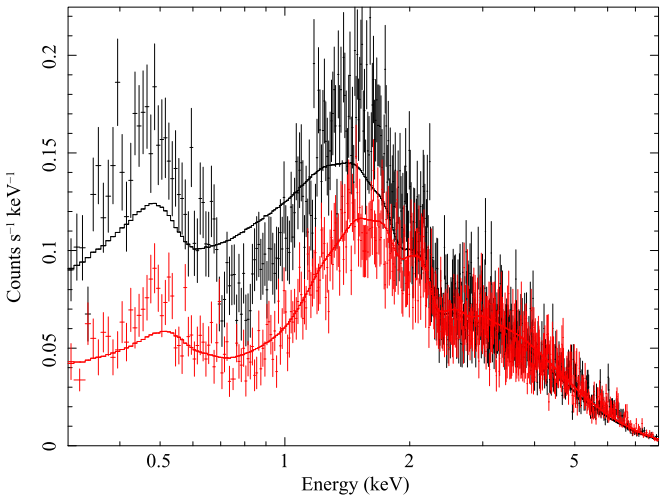

Figure 5. The *Swift* spectra fitted with a partial covering absorber model. This is clearly a poor fit compared to the models shown in Figures 3 and 4.

Table 4
Swift Spectra: PHASE Fit Parameters[b]

Spectrum	Log U	Log ($N_{\rm H}$/cm^{-2})	Photon Index[a] Γ
Anomaly	-0.3 ± 0.03	22.12 ± 0.01	1.42 ± 0.02
Pre-anomaly	-0.4 ± 0.01	22.18 ± 0.01	1.42 ± 0.02

Notes.
[a] Power-law parameters are tied for both the data sets.
[b] χ^2_ν for the joint fit is 1.1 for $\nu = 1003$ degrees of freedom.

Alternatively, the apparent soft "excess" could result from the recovery of the soft X-ray spectrum through a warm absorber. NGC 5548 is known to have an X-ray warm absorber, detected even in low-resolution spectra (e.g., Nandra et al. 1993; Mathur et al. 1995). We therefore tried to fit the *Swift* spectra with an absorbed power-law model modified by a warm absorber. We used PHASE (Krongold et al. 2003) to model the warm absorber. The parameters of this model are ionization parameter U, total column density $N_{\rm H}$, velocity v, and microturbulent velocity σ. Given the low resolution of the spectrum, we fixed v to match the galaxy redshift and σ was fixed to 200 km s^{-1}. Thus, the free parameters of the warm absorber model were U and $N_{\rm H}$. Once again, we fitted the two spectra simultaneously, keeping the power-law parameters tied. The fit was good ($\chi^2_\nu = 1.1$ for 1003 degrees of freedom) and the results of this fit are given in Table 4. The absorber $N_{\rm H}$ was found to be similar in the two spectra, and as expected, the

Table 5
NGC 5548 *Chandra* Observation Log

Obs.	ID	Date of Observation	JD	Exposure Time
I	15659	2014 Feb 3	2, 456, 692 (pre-anomaly)	5 ks
II	15660	2014 Mar 30	2, 456, 747 (just before anomaly)	5 ks
III	15661	2014 May 6	2, 456, 784 (during anomaly)	5 ks
IV	15662	2014 Jun 23	2, 456.832 (post-anomaly)	5 ks

warm absorber in the anomaly spectrum is more ionized (higher U), leading to the apparent excess in the soft X-ray band. The warm absorber column density, however, is unusually large ($\log N_{\rm H}$ (cm^{-2}) $\approx$ 22.2). The warm absorber column density in NGC 5548 has varied from about $\log N_{\rm H}$ (cm^{-2}) = 20.3 to $\log N_{\rm H}$ (cm^{-2}) = 21.7 (Mehdipour et al. 2015). While a significant increase in the column density is possible, it is also possible that the column density is actually lower, and there is an additional soft-excess component; we cannot distinguish between these two models. Warm absorbers with low ionization parameter are clearly related to UV absorption lines (e.g., Mathur et al. 1994, 1995, 1998; Monier et al. 2001; Krongold et al. 2003, 2005, 2007; Kaspi et al. 2004), so variability of the UV absorber (G. Kriss et al. 2017, in preparation) may help distinguish between the two possibilities. As noted below, in Section 4.2, the warm absorber model alone cannot explain the anomaly, so a variable warm absorber is unlikely to be the correct model of the soft excess.

As noted in Section 1, NGC 5548 was monitored intensively with *XMM-Newton* in 2013–2014. The source appeared in a highly obscured state then (Kaastra et al. 2014), with a column density $\sim 10^{23}$ cm^{-2}. In our STORM campaign, the absorption column density was over an order of magnitude lower ($\sim 10^{22}$ cm^{-2}). A detailed spectral analysis of *XMM-Newton* observations of NGC 5548 is presented by Cappi et al. (2016), who modeled the spectra with six different components: a power-law continuum; a cold reflection component; a soft thermal Comptonization emission model; a scattered emission-line component; a warm absorber; and up to two high column density partial covering "obscurers." Given the S/N of our *Swift* observations, it is not possible to fit the spectra with such a complex model and deduce meaningful information. Moreover, our interest is to understand the difference between the pre-anomaly and anomaly spectra. It is possible that the observed changes in the soft excess are caused by a combination of changes in multiple components. We cannot constrain these multiple components; instead, we have looked for a dominant model that describes the soft-excess variability. During the *XMM-Newton* campaign, the dominant variability component in the 0.3–0.8 keV range of soft excess was the covering fraction of the obscurer as reported by Mehdipour et al. (2016), but Cappi et al. (2016) show that the normalization of the Comptonization component was also important.

In our STORM campaign, the soft excess can be modeled as a BB, a warm absorber, a warm Comptonizing medium behind a thin veil of matter, or a combination of all these models; the *Swift* spectra cannot discriminate among these models. However, the dominant variability is not caused by the covering fraction or the column density of an absorber. As we discuss further in Section 4, the warm Comptonization model naturally explains several aspects of the UV anomaly, so this is our preferred model. While a change in the normalization of the warm Comptonization model can adequately describe the spectral difference between the pre-anomaly and anomaly spectra, our preferred model is of the change in the effective optical depth (Section 4). Thus, we see that the shape of the X-ray continuum changed during the anomaly phase, not just the normalization; this was clear from the model-independent spectra shown in Figure 1, and the spectral modeling confirms the same. Recently, Gardner & Done (2017) studied optical/UV variability of NGC 5548 and argued that a soft excess is required to understand the observed continuum lags; the observation of a soft excess with *Swift* and *Chandra* (Section 3) is consistent with this expectation.

3. *Chandra* Observations and Analysis

As a part of the *HST* campaign, we also observed NGC 5548 with the *Chandra* Low Energy Transmission Grating (LETG) and ACIS-S on four occasions from 2014 February to 2014 June for 5 ks each. The observation details are given in Table 5. The LETG was placed in front of the detector to avoid pile-up; obtaining high-resolution grating spectra was not the goal of these short 5 ks exposures. We analyzed the data using standard CIAO tools (version 4.7 and *caldb* version 4.6.7). All the observations were reprocessed using the *Chandra repro* task, which results in enhanced data quality and better calibration. We extracted the zeroth-order source and background spectra using the CIAO tool *specextract*, which also builds proper response (RMFs) and effective area (ARF) files required for analysis. We analyzed the spectra using both *XSPEC* and the CIAO fitting package *Sherpa*. We binned the spectra to 25 counts minimum per channel using *ftool grppha*.

It was clear that in the hard X-ray band (2–8 keV) the spectra are very similar, but at softer energies they show differences, similar to what we found in *Swift* spectra. Thus, we fit the *Chandra* spectra with an absorbed power-law model, as we did for *Swift* spectra, with the results shown in Figure 6. Once again we see that there is a clear soft excess in *Chandra* observations II (day 57 = JD 2, 456, 747) and III (day 93 = JD 2, 456, 784), which were taken just before and during the anomaly. Observations I and IV took place when the source was in its normal state, and they show no soft excess. The appearance of the soft excess in observations II and III once again suggests that it may be related to the anomaly.

We fit the *Chandra* spectra with the same series of models discussed above, primarily to determine if they are consistent with the *Swift* results despite their lower S/N. The models that fit the *Swift* data well also fit the the *Chandra* data well, and the partial covering power-law model is a poor model of the *Chandra* spectra as well ($\chi^2_\nu = 2.32$ for $\nu = 63$ degrees of freedom), with the fit yielding a covering fraction of unity.

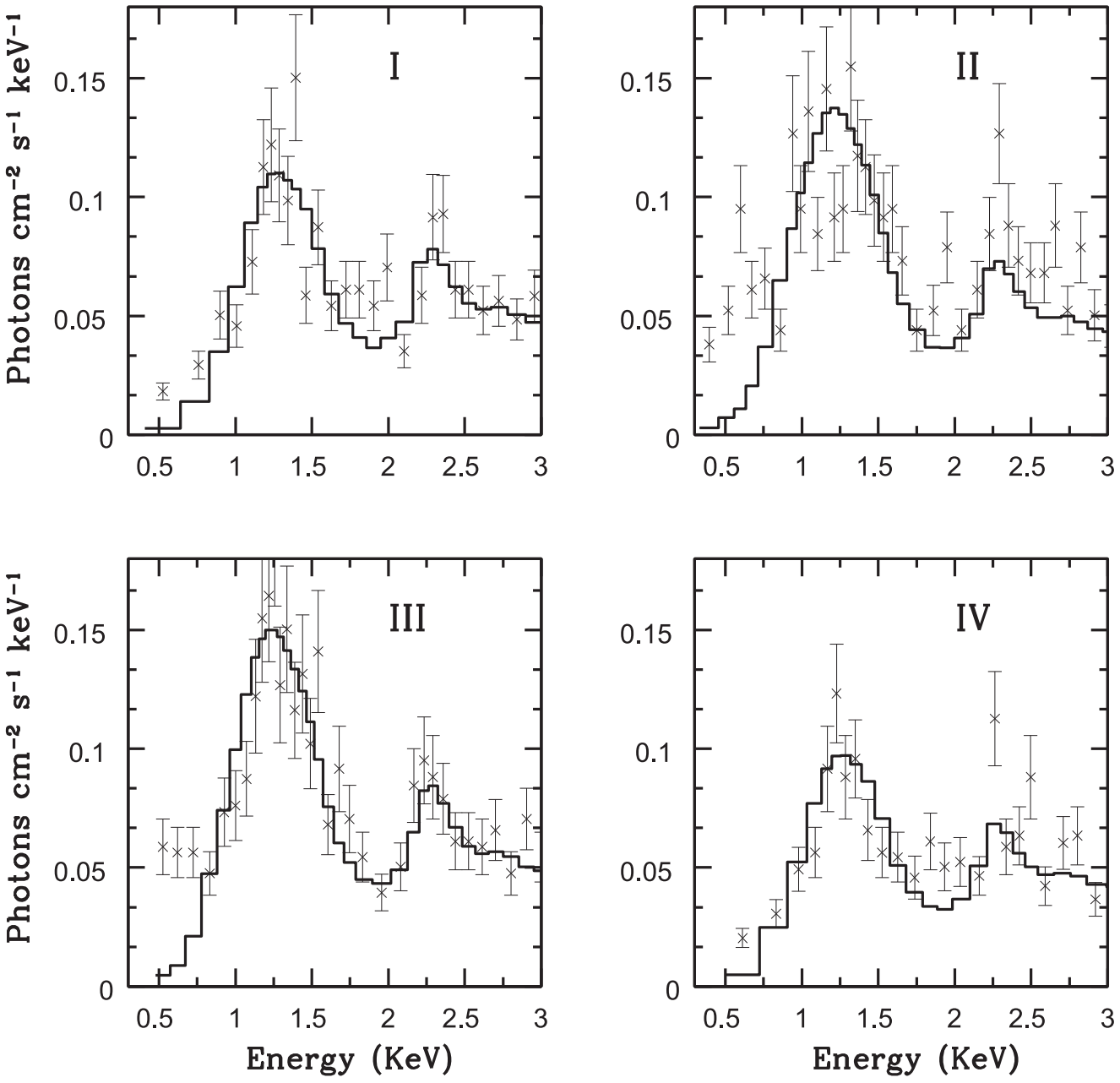

Figure 6. *Chandra* spectra with the best-fit absorbed power-law model. The soft excess is apparent in observations II and III.

4. Results

4.1. Soft-excess

Ever since the discovery of soft X-ray excesses (Singh et al. 1985), there has been a debate about their origin and physical nature. The possible explanations have been narrowed down to (1) reflection of the hard X-ray source by the accretion disk (e.g., Crummy et al. 2006); (2) an additional Comptonizing medium around the accretion disk (e.g., Ross et al. 1992); or (3) thermal emission from an accretion disk. Understanding the nature of the soft excess is important because of its potentially large luminosity and because it is an integral part of the accretion process. Though no correlation has been found between the strength of the soft-excess and the black hole mass or its luminosity (e.g., Bianchi et al. 2009), multiwavelength studies have revealed a possible correlation of the UV slope with the soft-excess strength and shape (e.g., Walter & Fink 1993; Atlee & Mathur 2009). From the multiwavelength campaign studying Mrk 509, Mehdipour et al. (2011) found that the soft X-ray excess is correlated with the thermal optical-UV emission from the accretion disk and is not correlated with the 2–10 keV X-ray power law. This favors Comptonization of UV/optical photons by a hot plasma for the origin of the soft excess.

In NGC 5548, the soft excess was previously detected in 2000 during an unobscured period, but the source was heavily absorbed during 2013 (Kaastra et al. 2014) and the soft-excess was modeled as a Comptonized corona (Mehdipour et al. 2015). The soft excess observed during our campaign is well modeled as a BB (an optically thick corona would emit like a

BB), but the anomaly is better explained by the warm Comptonization model, as discussed below, so this is our preferred explanation.

4.2. Understanding the UV Anomaly

The X-ray spectra provide a possible explanation for the UV anomaly. First, the X-ray spectra rule out variable absorption as the cause of the anomaly. If anything, the absorption was lower during the anomaly. It is possible that the EUV ionizing continuum source was obscured, while the X-ray source was not, but that is unlikely since the X-ray continuum source size in AGNs appears to be smaller than that of the UV/EUV (e.g., Mosquera et al. 2013). Partial covering of the continuum fits the data poorly and is unlikely to be the cause of the anomaly.

The second important fact is that the UV emission-line flux decreased during the anomaly. This suggests that the EUV ionizing continuum flux decreased during the anomaly (as discussed in Paper IV; the ionization potential of C III is 47.9 eV and that of Si III is 33.5 eV). This cannot be explained by a change in the warm absorber because the warm absorber in the anomaly spectrum is more ionized (higher U), requiring an increase in the EUV continuum during the anomaly. Thus, our preferred scenario is that of the intrinsic change in the soft X-ray spectrum.

The observed changes can be naturally explained by the warm Comptonization model. In this model, the UV disk photons are Compton upscattered to soft X-ray energies by the optically thick corona. In a normal situation, where the UV and soft X-ray fluxes are correlated, higher UV flux leads to more input photons for Comptonization, so more soft X-rays; we can describe this as a change in the normalization of the model. What we have, however, is the opposite situation during the anomaly: the EUV flux decreases, while the soft X-ray flux increases. Perhaps the EUV photons are depleted from the flux seen by the BLR, but are Comptonized into soft X-rays. This could be due to either a true change in the optical depth or an increase in the region covering the UV/EUV-emitting region, which could be considered an increase in the "effective optical depth" of the corona. The BLR is then deprived of the ionizing photons, so the emission-line and UV continuum variability are decoupled (the "anomaly"). The increase in the effective optical depth in the anomaly spectrum is $\Delta\tau = 1.8$, implying a reduction in the EUV flux by approximately $e^{-\Delta\tau}$ or 16.5%. Interestingly, the observed deficit in the C IV broad emission-line flux during the anomaly is of a similar amplitude (Figure 1 (e) and 2 in Paper IV).

Thus, the warm Comptonization model can simultaneously explain all three observations (the UV emission-line flux decrease, the soft-excess increase, and the emission-line anomaly), so it is our preferred model. We do not understand why the corona may change its physical structure in this way; observations such as these provide motivations for further theoretical work on the structure of the accretion disk and the corona. Notably, an anomalous continuum behavior has been seen before. In 3C 273, there was one epoch of *XMM-Newton* observations when the UV flux decreased but the X-ray flux increased (Page et al. 2004), while the source otherwise behaved normally.

5. Conclusion

In this paper, we report on analyses of *Swift* and *Chandra* X-ray spectra taken during the *HST* monitoring campaign of NGC 5548 that help us understand the UV anomaly reported in Paper IV. We show that obscuration of the continuum source is unlikely to be the cause of the anomaly. Instead, the spectral energy distribution of the continuum changed during the anomaly, as seen in the X-ray spectra. A possible scenario may be that the warm Comptonizing corona covered more of the accretion disk during the anomaly, depleting EUV photons, while increasing the soft X-ray excess. The decrease in the ionizing continuum then leads to the emission-line anomaly. In order to understand the finer details of the anomaly, detailed photoionization models will be necessary. These results demonstrate the importance of contemporaneous X-ray spectra to interpreting high-quality RM data. We suggest that future RM campaigns in the optical and/or UV include an X-ray component as well.

We are grateful to Christine Done for discussions on the warm Comptonization model. Support for this work was provided by the National Aeronautics and Space Administration (NASA) through *Chandra* Award Number G04-15114X to S.M. issued by the *Chandra* X-ray Observatory Center, which is operated by the Smithsonian Astrophysical Observatory for and on behalf of NASA under contract NAS8-03060. Support for *HST* program GO-13330 was provided by NASA through a grant from the Space Telescope Science Institute, which is operated by the Association of Universities for Research in Astronomy, Inc., under NASA contract NAS 5-26555. C.S.K. is supported in part by NSF grants AST-1515876 and AST-1515927. K.H. acknowledges support from STFC grant ST/M001296/1. K.L.P. and P.A.E. ackowledge support from the UK Space Agency. A.V.F.'s group at UC Berkeley is grateful for financial assistance from NSF grant AST-1211916, the TABASGO Foundation, and the Christopher R. Redlich Fund. Y.K. acknowledges support from the grant PAIIPIT IN104215 and CONACYT grant168519. This work made use of data supplied by the UK Swift Science Data Centre at the University of Leicester (see Evans et al. 2009).

ORCID iDs

K. Page https://orcid.org/0000-0001-5624-2613
R. W. Pogge https://orcid.org/0000-0003-1435-3053
M. R. Goad https://orcid.org/0000-0002-2908-7360
A. J. Barth https://orcid.org/0000-0002-3026-0562
T. G. Beatty https://orcid.org/0000-0002-9539-4203
S. Bisogni https://orcid.org/0000-0003-3746-4565
T. A. Boroson https://orcid.org/0000-0001-9481-1805
W. N. Brandt https://orcid.org/0000-0002-0167-2453
A. A. Breeveld https://orcid.org/0000-0002-0001-7270
C. T. Coker https://orcid.org/0000-0002-9954-7887
D. M. Crenshaw https://orcid.org/0000-0002-6465-3639
K. V. Croxall https://orcid.org/0000-0002-5258-7224
A. J. Deason https://orcid.org/0000-0001-6146-2645
M. Eracleous https://orcid.org/0000-0002-3719-940X
A. V. Filippenko https://orcid.org/0000-0003-3460-0103
O. D. Fox https://orcid.org/0000-0003-2238-1572
C. J. Grier https://orcid.org/0000-0001-9920-6057
D. Grupe https://orcid.org/0000-0002-9961-3661
E. Holmbeck https://orcid.org/0000-0002-5463-6800
D. Horenstein https://orcid.org/0000-0002-0698-6013
Keith Horne https://orcid.org/0000-0003-1728-0304
M. Im https://orcid.org/0000-0002-8537-6714
P. L. Kelly https://orcid.org/0000-0003-3142-997X
J. A. Kennea https://orcid.org/0000-0002-6745-4790

C. S. Kochanek https://orcid.org/0000-0001-6017-2961
K. T. Korista https://orcid.org/0000-0003-0944-1008
G. A. Kriss https://orcid.org/0000-0002-2180-8266
M. W. Lau https://orcid.org/0000-0001-9755-9406
M. A. Malkan https://orcid.org/0000-0001-6919-1237
R. McGurk https://orcid.org/0000-0003-2064-4105
D. Mudd https://orcid.org/0000-0003-2371-4121
H. Netzer https://orcid.org/0000-0002-6766-0260
A. Pancoast https://orcid.org/0000-0003-1065-5046
A. Pizzella https://orcid.org/0000-0001-9585-417X
J.-U. Pott https://orcid.org/0000-0003-4291-2078
H.-W. Rix https://orcid.org/0000-0003-4996-9069
D. A. Saylor https://orcid.org/0000-0002-0558-1305
J. S. Schimoia https://orcid.org/0000-0002-5640-6697
B. J. Shappee https://orcid.org/0000-0003-4631-1149
I. Shivvers https://orcid.org/0000-0003-3373-8047
A. Skielboe https://orcid.org/0000-0001-9765-3603
M. Spencer https://orcid.org/0000-0003-1240-1939
J. Tayar https://orcid.org/0000-0002-4818-7885
M. Vestergaard https://orcid.org/0000-0001-9191-9837
S. Villanueva Jr. https://orcid.org/0000-0001-6213-8804
C. Villforth https://orcid.org/0000-0002-8956-6654

References

Atlee, D. W., & Mathur, S. 2009, ApJ, 703, 1597
Bianchi, S., Guainazzi, M., Matt, G., Fonseca Bonilla, N., & Ponti, G. 2009, A&A, 495, 421
Cappi, M., De Marco, B., Ponti, G., et al. 2016, A&A, 592, 27
Crummy, J., Fabian, A. C., Gallo, L., & Ross, R. R. 2006, MNRAS, 365, 1067
De Rosa, G., Peterson, B. M., Ely, J., et al. 2015, ApJ, 806, 128 (Paper I)
Dicky, J. M., & Lockman, F. J. 1990, ARA&A, 28, 215
Edelson, R., Gelbord, J. M., Horne, K., et al. 2015, ApJ, 806, 129 (Paper II)
Evans, P., Beardmore, A. P., Page, K. L., et al. 2009, MNRAS, 397, 1177
Fausnaugh, M., Denney, K. D., Barth, A. J., et al. 2016, ApJ, 821, 56 (Paper III)
Gardner, E., & Done, C. 2017, arxiv:1603.09564
Goad, M., Korista, K. T., De Rosa, G., et al. 2016, ApJ, 824, 11 (Paper IV)
Kaastra, J., Kriss, G. A., Cappi, M., et al. 2014, Sci, 345, 64
Kaspi, S., Netzer, H., Chelouche, D., et al. 2004, ApJ, 611, 68
Krongold, Y., Nicastro, F., Brickhouse, N. S., et al. 2003, ApJ, 597, 832
Krongold, Y., Nicastro, F., Brickhouse, N. S., Elvis, M., & Mathur, S. 2005, ApJL, 622, L842
Krongold, Y., Nicastro, F., Elvis, M., et al. 2007, ApJ, 659, 1022
Mathur, S., Elvis, M., & Wilkes, B. 1995, ApJ, 452, 230
Mathur, S., Wilkes, B., & Elvis, M. 1998, ApJL, 503, L23
Mathur, S., Wilkes, B., Elvis, M., & Fiore, F. 1994, ApJ, 434, 493
Mehdipour, M., Branduardi-Raymont, G., Kaastra, J. S., et al. 2011, A&A, 534, 39
Mehdipour, M., Kaastra, J. S., Kriss, G. A., et al. 2015, A&A, 575, 22
Mehdipour, M., Kaastra, J. S., Kriss, G. A., et al. 2016, A&A, 588, 139
Monier, E., Mathur, S., Wilkes, B., & Elvis, M. 2001, ApJ, 559, 675
Mosquera, A., Kochanek, C., Chen, B., et al. 2013, ApJ, 769, 53
Nandra, K., Fabian, A. C., George, I. M., et al. 1993, MNRAS, 260, 504
Page, K., Turner, M. J. L., Done, C., et al. 2004, MNRAS, 349, 57
Pei, L., Fausnaugh, M. M., Barth, A. J., et al. 2017, ApJ, 837, 131 (Paper V)
Pounds, K. A., Reeves, J. N., Page, K. L., et al. 2003, MNRAS, 341, 953
Ross, R. R., Fabian, A. C., & Mineshige, S. 1992, MNRAS, 258, 189
Singh, K. P., Garmire, G. P., & Nousek, J. 1985, ApJ, 297, 633
Starkey, D., Horne, K., Fausnaugh, M. M., et al. 2017, ApJ, 835, 65 (Paper VI)
Walter, R., & Fink, H. H. 1993, A&A, 274, 105